

Optical observations of the young supernova remnant SNR 0540-69.3 and its pulsar[★]

N. I. Serafimovich^{a,b}, P. Lundqvist^b, Yu. A. Shibano^a, J. Sollerman^b

^a*Ioffe Physical Technical Institute, Politekhnikeskaya 26, St. Petersburg, 194021, Russia*

^b*Stockholm Observatory, AlbaNova Science Center, Department of Astronomy, SE-106 91 Stockholm, Sweden*

Abstract

We have used the ESO NTT/EMMI and VLT/FORS1 instruments to examine the LMC supernova remnant 0540-69.3 as well as its pulsar (PSR B0540-69) and pulsar-powered nebula in the optical range. Spectroscopic observations of the remnant covering the range of 3600 – 7350 Å centered on the pulsar produced results consistent with those of Kirshner et al. (1989), but also revealed many new emission lines. The most important are [Ne III] $\lambda\lambda$ 3869, 3967 and Balmer lines of hydrogen. In both the central part of the remnant, as well as in nearby H II regions, the [O III] temperature is higher than $\sim 2 \times 10^4$ K, but lower than previously estimated. For PSR B0540-69, previous optical data are mutually inconsistent: HST/FOS spectra indicate a significantly higher absolute flux and steeper spectral index than suggested by early time-resolved groundbased UBVR photometry. We show that the HST and VLT spectroscopic data for the pulsar have $\gtrsim 50\%$ nebular contamination, and that this is the reason for the previous difference. Using HST/WFPC2 archival images obtained in various bands from the red part of the optical to the NUV range we have performed an accurate photometric study of the pulsar, and find that the spectral energy distribution of the pulsar emission has a negative slope with $\alpha_\nu = 1.07_{-0.19}^{+0.20}$. This is steeper than derived from previous UBVR photometry, and also different from the almost flat spectrum of the Crab pulsar. We also estimate that the proper motion of the pulsar is 4.9 ± 2.3 mas yr⁻¹, corresponding to a transverse velocity of 1190 ± 560 km s⁻¹, projected along the southern jet of the pulsar nebula.

Key words: supernova remnants – pulsars – spectroscopy – photometry – astrometry – supernova remnants: individual: SNR 0540-69.3 – pulsars: individual: PSR B0540-69.3

1. Introduction

Supernova remnant (SNR) 0540-69.3 (henceforth simply 0540) has been observed at wavelengths ranging from X-rays to the radio. Both in

the radio (1) and in X-rays (2; 3), the remnant is bounded by an outer shell, which has a radius of at least $\sim 30''$. Inside the outer shell, the emission from the remnant is concentrated to a substantially smaller nebula (4; 5). In [O III] ($\lambda = 5007$ Å), the diameter is $\sim 8''$ (henceforth we will refer to this as the ‘central part of the SNR’ (SNRC)). In this and other lines, the emission appears to mainly come from a few blobs and filaments. The

[★] Based on observations performed at the European Southern Observatory, La Silla and Paranal, Chile (ESO Programmes 56.C-0731 and 67.D-0519).

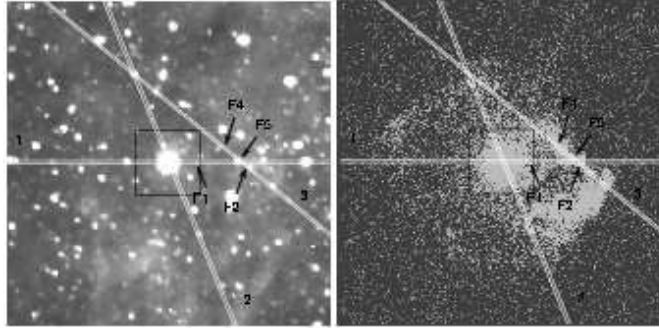


Fig. 1. A $100'' \times 100''$ field around 0540. The left panel is an optical image obtained with the ESO NTT in a narrow band filter centered on the [O III] ($\lambda = 5007 \text{ \AA}$) emission line, and the right panel shows an X-ray image obtained with Chandra in the 1.5–6.4 keV range. White parallel lines marked by numbers show the slit positions used in our spectroscopic observations of the SNRC with the NTT (slit 2) and VLT (slits 1 and 3). The areas marked “F1, F2, F4, F5” show the positions of several emission-line regions identified from the spectroscopic observations and described in detail in (16). A $20'' \times 20''$ box marks the inner region of the remnant enlarged in Fig. 2.

SNRC also emits an optical continuum, believed to be synchrotron emission from the pulsar wind nebula (PWN) (9; 10). Such a nebula is expected since the remnant harbors the young pulsar PSR B0540-69 which is observed to emit in X-rays (6), in the optical (7), and in the radio (8). The SNRC with its pulsar bears many similarities to the Crab Nebula, which is why 0540 is sometimes referred to as the Crab’s twin. A detailed comparison of PSR B0540-69 with the Crab pulsar and its PWN can be found in (10).

The spectrum of the SNRC is dominated by forbidden oxygen and sulphur lines. From the strong oxygen lines it has been classified as an “oxygen-rich SNR” (OSNR). This class of objects has a handful of members, of which Cas A is the most studied object (e.g., (11) and references therein). However, Cas A is not pulsar-powered, although a point-like X-ray source has been detected near its center (12). Thus 0540 is an interesting link between pulsar-powered remnants and OSNRs. Here we present some new results for this object obtained with the ESO NTT and VLT, and with the HST.

2. Observations

Observations of 0540 were performed on 1996 January 17, using the ESO NTT telescope with the ESO Multi-Mode Instrument (EMMI)¹. Narrow-band images in [O III] ($\lambda = 5007 \text{ \AA}$) were obtained using a zero velocity [O III]/0 filter² and an exposure time of 30 minutes. The pixel size was $0''.268$. We also carried out low-resolution ($2.3 \text{ \AA}/\text{pixel}$) long-slit spectroscopy of 0540 in the 3850–8450 \AA range. The [O III]/0 image is shown in Fig. 1 (*left*), where we also show the slit position of the NTT spectral observation (marked by “2”). Further spectroscopic observations were carried out in the 3600–6060 \AA range on 2002 January 9 and 10 with the ESO VLT telescope using the FOcal Reducer/low dispersion Spectrograph 1 (FORs1)³ with a dispersion of $1.18 \text{ \AA}/\text{pixel}$, and a spatial scale of $0''.2$ per pixel. Total exposure times of 154 and 132 minutes were used for the two slit positions, marked by “1” and “3” in Fig. 1, respectively. Slits 1 and 2 were chosen to include the SNRC and the pulsar. Slit 3 does not cross the SNRC, but was placed to probe emission from the outer shell in a region where it is most

¹ <http://www.lis.eso.org/lasilla/Telescopes/NEWNT>

² <http://www.lis.eso.org/lasilla/Telescopes/NEWNT/emmi/emmiFilters.html>

³ <http://www.eso.org/instruments/fors1/>

clearly identified in the Chandra X-ray image (13) (Fig. 1, right). The Chandra image in Fig. 1 was obtained on 1999 November 22 with the ACIS-S in the 1.5 – 6.4 keV range with a spatial resolution of $0''.492$ per pixel using a total exposure time of 27.8 ks. All spectroscopic observations were performed using a slit width of $1''$ and the seeing was generally about $1''$.

The 0540 field has also been imaged with the HST/WFPC2 on several occasions in various bands. Data for observations through the F336W, F502N, F547M, F673N and F791W filters were obtained on 1999 October 17 using total exposure times of 600 s, 11000 s, 800 s, 8200 s and 400 s, respectively (14). Data in the narrow band F658N and wide band F555W filters were obtained on 1995 October 19 with 4000 s, and 600 s exposures, respectively (15). We retrieved these images from the HST archive and used them in our analysis. The SNRC was exposed on the Planetary Camera (PC) chip with a spatial resolution of $0''.046$ per pixel revealing the pulsar and the structure of its PWN (Fig. 2), as well as the fine structure of the SNRC and its neighborhood. All the data obtained have been reduced and calibrated in a standard way (for details see (10; 16)).

3. Results

3.1. Spectroscopy of the central part of 0540.

Spectroscopic studies of the SNRC were carried out in detail by Kirshner et al. (1989) (17) using a larger slit width ($1''.5$) and at a different position angle. To compare our results with theirs, we extracted 1D spectra of the SNRC from our spectral images using the IRAF procedure `apall` and spatial extents of $10''$ and $8''$ centered on the pulsar for slits “1” and “2”, respectively. The extracted windows correspond to the observed extents of the SNRC along the respective slit directions. The extracted VLT spectrum from slit 1 shown in Fig. 3 is consistent with that of Kirshner et al. (17). However, the higher sensitivity and spectral resolution of the VLT observations also allow us to find many new lines not previously detected. The most important

findings are [Ne III] $\lambda\lambda 3869, 3967$ and Balmer lines of hydrogen all the way down to H I $\lambda 3889$. These lines are marked in Fig. 3 and detected at least at $\geq 5\sigma$ significance level. They belong to the SNR material, and not to the LMC background, since the measured shifts of their line centroids correspond to a velocity of $500 - 800 \text{ km s}^{-1}$, which is consistent with the velocities of the much stronger [O III] and [S II] lines. Moreover, the lines are velocity broadened to the same extent (a typical width is $\sim 2000 \text{ km s}^{-1}$) as other lines emitted by the remnant. While the neon lines can be used to derive an O/Ne ratio which in turn constrains the progenitor mass (cf. (16)), the Balmer lines show that the previously detected emission around H α is at least partly due to H α , and not only to [N II] $\lambda 6583$ or any other line as previously discussed (15; 17).

3.2. SNRC density from [S II] $\lambda\lambda 6716, 6731$.

The intensity ratio $R_{[\text{S II}]} = \frac{I(\lambda 6716)}{I(\lambda 6731)}$ is sensitive to the electron number density, N_e (e.g., (19)). As discussed in (16), the two components of [S II] detected using slit 2, blend together because of the velocity broadening of the emitting gas in 0540. There are, however, a few positions along the slit for which a deblending is possible. From various fits to the line profiles at these positions, we obtained $R_{[\text{S II}]} \approx 0.7 \pm 0.1$. To estimate the density, we used the multilevel model for S II described in (20), but with atomic data further updated according to (21). Adopting the above $R_{[\text{S II}]}$ value we obtain $N_e = (1.4 - 4.3) \times 10^3 \text{ cm}^{-3}$ assuming the temperature $T = 10^4 \text{ K}$ and $N_e = (1.8 - 5.3) \times 10^3 \text{ cm}^{-3}$ at $T = 2 \times 10^4 \text{ K}$. The lower temperature is probably more likely considering our findings for [O III] (see below), so a reasonable density range is $N_e = (1 - 5) \times 10^3 \text{ cm}^{-3}$. This is similar to the density in the Crab Nebula for which [O II] and [S II] line ratios indicate electron densities in the range of $4 \times 10^2 - 4 \times 10^3 \text{ cm}^{-3}$ for various filaments observed (22).

3.3. SNRC temperature from [O III].

As can be seen from Fig. 3, [O III] $\lambda 4363$ is clearly detected in the spectrum of the SNRC of

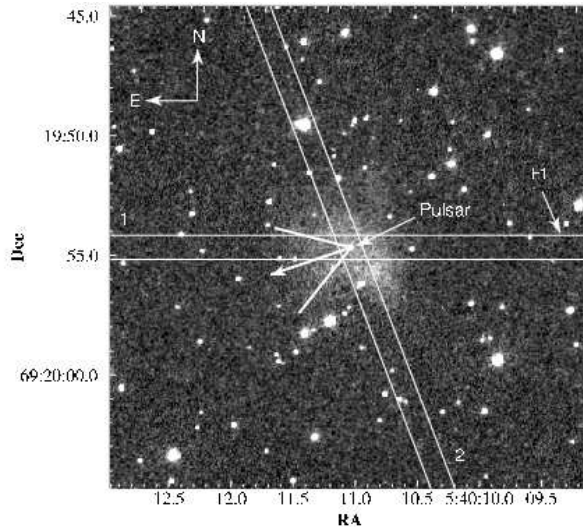


Fig. 2. A $20'' \times 20''$ HST/WFPC2 image of the inner region of 0540 in the F547M band. Slit positions 1 and 2 shown in Fig. 1, as well as the position of the pulsar and the emission-line filament F1 are marked. The slit widths are $1''$. The diffuse emission surrounding the pulsar comes from the PWN. Note its elongation in the NE-SW direction. The proper motion of the pulsar is in the south-east direction, and its 1σ – angular uncertainties are shown by the thick arrow and lines (see text). Coordinates refer to epoch J2000.

0540. This enables us to estimate the temperature from the flux ratio $R_{[\text{O III}]} = \frac{I(\lambda\lambda 4959, 5007)}{I(\lambda 4363)}$, (e.g., (19)). A complication for 0540 is, however, that lines from the SNRC are blended due to velocity broadening. In particular, $[\text{Ne III}] \lambda\lambda 3869, 3967$ and $[\text{O III}] \lambda 4363$ are contaminated by H I lines. This leads to an underestimate of $R_{[\text{O III}]}$, and consequently an overestimate of the temperature if deblending is not made. To deblend these lines we used $\text{H}\beta$ as a template profile for all H I lines. Incorporating a six-level model atom for O III from (26) gives $T_e \approx 2.4 \times 10^4$ K (for the electron density we found above from $[\text{S II}]$). Although our $[\text{O III}]$ temperature is significantly lower than that of (17), who estimated $T_e \sim 3.4 \times 10^4$ K without taking deblending into account, it is still much higher than in normal H II regions. The corresponding temperature in the Crab Nebula is in the range $(1.1 - 1.8) \times 10^4$ K (22), and is thought to mainly arise from photoionization heating (17). Our value of T_e from $[\text{O III}]$ may point in the direction of shock heating not being the sole source of heating of the SNRC of 0540 since photoionization by a hard spectrum, like in the Crab, can also give

rise to high $[\text{O III}]$ temperatures (e.g., (17)). Modeling is needed to sort out which source of heating dominates in the SNRC of 0540.

3.4. 0540 filaments.

0540 is near the LMC H II region DEM 269 and the OB association LH 104 (17). This is reflected in our spectroscopic images which contain strong, narrow emission lines that vary spatially in strength along the slits. These lines are significantly narrower (actually unresolved) than the lines from the SNRC of 0540. To study whether or not some of the H II (or at least emission-line) regions are affected by the SNR activity, we selected several filaments detected along our slits and analyzed their spectra. Many of the filaments actually do show highly ionized ions (as mainly deduced from iron) as expected for regions close to the X-ray emitting parts of the remnant. The filaments we studied in greater detail were along the VLT slits “1” and “3”, and they are marked F1, F2, F4, F5 in Fig. 1. For reference we also looked at a filament (named F3) which in projection is situated

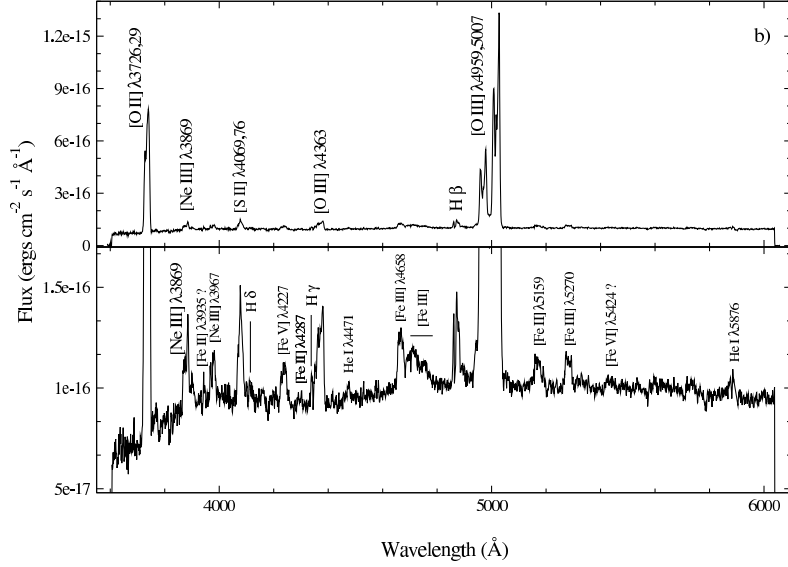


Fig. 3. *Top*: The ESO VLT slit 1 spectrum of the central part of 0540 (marked “b”). *Bottom*: Same spectrum but with an expanded flux scale to highlight weaker lines. The spectrum has been dereddened using $E(B - V) = 0.20$ and $R=3.1$. The high signal-to-noise ratio of the VLT spectrum made it possible to detect faint lines from the SNRC.

1/4 from the pulsar (to the east, and outside the region shown in Fig. 1). While F3 can still be affected by the radiation field of 0540, it clearly cannot be shock excited by the remnant.

Filament F1, which in projection is the closest one to the SNRC, is remarkably hot, $T_e \sim 3.7 \times 10^4$ K. Filaments F2, F4 and F5 are closer to the outer shock front detected in X-rays (as seen in projection), and they all have temperatures in excess of 2.3×10^4 K. The reference filament F3 has an [O III] temperature of $\sim 1.7 \times 10^4$ K. The temperatures of all filaments (even that of F3) are substantially higher than in normal H II regions. Despite the fact that LMC is less metal-rich than the Milky Way, and metal line cooling in H II regions is therefore expected to be less efficient there, typical [O III] temperatures in, e.g., the 30 Doradus region vary rather mildly (± 140 K) from the average value of 10270 K (27). The high temperature of filaments F1-F5 around the SNRC of 0540 suggests that they are all affected by the remnant.

The spectral resolution of our FORS1 observations is ~ 180 km s $^{-1}$ at [O III] $\lambda 5007$ Å, but the line center of the filament lines can be determined to within a fraction of this (~ 20 km s $^{-1}$) for the strongest lines. Taking filament F3 as a reference, all the other filaments around 0540 are consistent with having their line center velocities within this ± 20 km s $^{-1}$ uncertainty range. In the young remnant of SN 1987A, the shocked gas in the inner ring has displacements that are marginally larger than 20 km s $^{-1}$ (28), but the effect is certainly not large enough for us to rule out shocks as the excitation mechanism for the 0540 filaments. SN 1987A also shows that the draping of the blast wave around the ring clumps produces line profiles with widths that are in excess of the spectral resolution of our 0540 observations. This may pose a stronger constraint on the shock hypothesis for the 0540 filaments than the lack of line displacement, as we do not see any broadening (beyond the instrumental broadening) of the 0540 filament lines (16). We note, however,

that both the line displacement and the line broadening are geometry dependent, and the geometry may certainly be less extreme in the 0540 filaments than in the ring clumps of SN 1987A. A shock imprint on the emission lines may therefore be less obvious for 0540 than for SN 1987A. An alternative, or maybe complementary, excitation scenario for filaments F1, F2, F4 and F5 around 0540 is that they are photoionized by a time-varying EUV/X-ray source. It was shown in (20) that [O III] temperatures of several times 10^4 K can be attained in such a case. The ionizing source could in this case be naturally provided by the X-rays created when the blast wave overtakes 0540 filaments. Modeling to test the photoionization scenario is in progress (16). Observations with better spectral resolution will also help to resolve the excitation mechanism.

3.5. *The spectral energy distribution of the pulsar emission.*

PSR B0540-69.3 is one of a few pulsars for which a near-UV and optical spectrum has been reported. Hill et al. (23) obtained a time-integrated near-UV spectrum with HST/FOS and Middleditch et al. (24) used time-resolved photometry to establish a broadband ground-based UBVRI ‘spectrum’ in the optical. These two investigations show, however, a significant difference in the absolute flux in the spectral range where they overlap. To check this mismatch we used two recent sets of data, one is our VLT/FORS spectroscopy of 0540, and the other is the HST/WFPC2 imaging (15; 14). Our spectroscopic and photometric results are shown in Fig. 4 (10). Considered separately, they are in good agreement with previous results. However, they do not erase the significant discrepancy between the spectroscopic and photometric data sets, which is much larger than the statistical uncertainties of our measurements. The only plausible explanation to this discrepancy is that the HST/FOS spectroscopy is strongly contaminated by the PWN. As an additional test we measured the pulsar flux in the F336W, F547M, F555W, and F791W bands, using a circular aperture with a radius of 10 PC-pixels (total diameter of $0''.92$) centered on the pulsar, without subtraction of the background. These

conditions reproduce the parameters of the spectral measurements within a circular aperture of almost the same diameter ($0''.86$) made with the HST/FOS by Hill et al. 1997 (23). The 10-pixel fluxes are much closer to the HST and VLT spectral fluxes. We estimate that within a 10 pixel radius, the PWN contributes at least 50%. This can also be seen by comparing our accurate pulsar photometry with our 10 pixel test (10). We conclude that the previously published spectral data on the pulsar emission cannot be considered as reliable. Our broadband HST ‘spectrum’ (or rather broadband spectral energy distribution) of the pulsar, where the background from the nebula has been accurately subtracted off, can be considered as a fair estimate of the pulsar spectral energy distribution. It has a nonthermal origin and is described by a power law, $F_\nu \propto \nu^{-\alpha}$, with the spectral index $\alpha_\nu = 1.07^{+0.20}_{-0.19}$, while that of Middleditch et al. has $\alpha_\nu = 0.33 \pm 0.45$ using updated dereddening corrections. The flatter spectrum of Middleditch et al. (24) is partially due to a spectral jump upwards for the U band that could be due to a systematic flux error in this band.

3.6. *Proper motion of PSR B0540-69.3.*

The position of PSR B0540-69.3 is defined on the HST PC chip frames with an accuracy of better than 0.17 PC pixels which corresponds to $0''.0077$. This allows a direct estimate of the proper motion of the pulsar using an accurate superposition of the F555W and F547M images taken at epochs separated by 3.995 years. Using the positions of 9 reference stars to construct the coordinate transformation between the two images, we find a proper motion $\mu = 4.9 \pm 2.3$ mas yr $^{-1}$ in the South-East direction (see Fig. 2) at a position angle of $109^\circ \pm 33^\circ$ (projected along the southern jet of its PWN). The significance of this result is low and can be considered only as an attempt to make a first direct measurement of the proper motion. Based on the displacement between the pulsar optical position and the center of the PWN, as seen in radio, Manchester et al. 1993b (1) argued for a similar value of the proper motion but in the South-West direction (in the plane of the

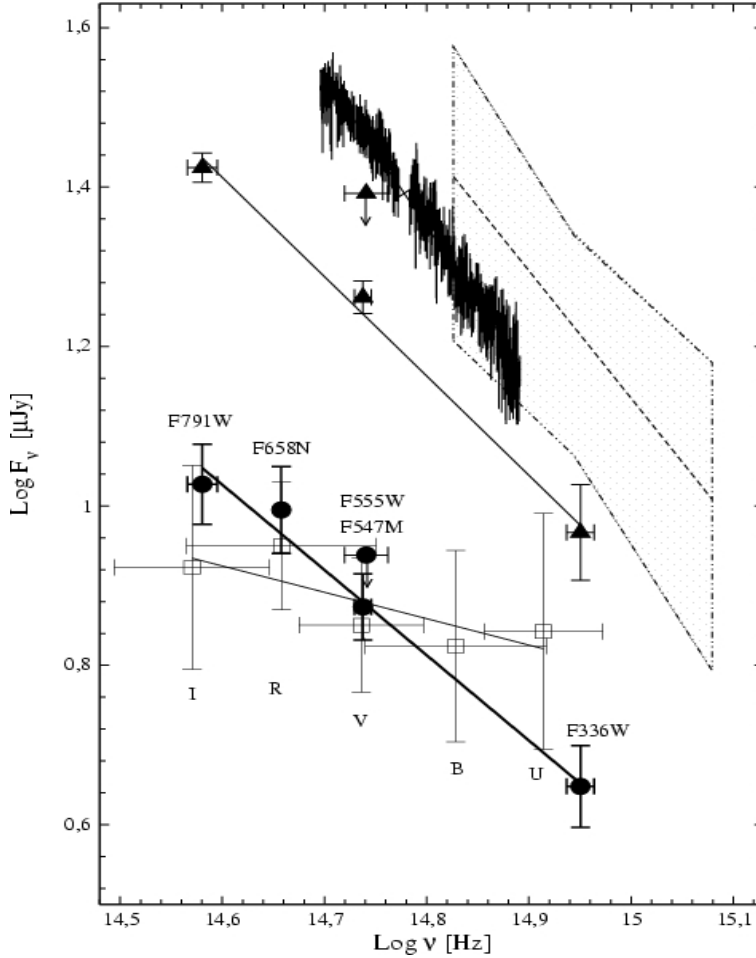


Fig. 4. The optical spectrum of PSR B0540-69.3 obtained with different telescopes and instruments. The uppermost is the VLT slit 1 spectrum for the 6-pixel area centered at the pulsar. The bright [O III] nebular lines have been removed. The dashed line and the hourglass-shaped error-box show a power law fit and 1σ -uncertainties of the UV spectrum obtained by Hill et al. (1997). Filled triangles show the HST photometry with a 10-pixel circular aperture to compare with the above spectra. Filled ellipses show our HST photometric results, see (10). Open rectangles are the photometric UBVR data from Middleditch et al. (1987). All data are dereddened using $E(B - V) = 0.20$. Solid lines show power-law fits to the HST and Middleditch photometric data sets.

PWN torus, as seen in projection). We note that the proper motion of the Crab pulsar is projected along the symmetry axis of the inner Crab nebula, as defined by the direction of the PWN jet discovered by ROSAT, and that a similar situation applies to the Vela pulsar (25). If our estimates are confirmed, we have the intriguing situation that all these three young pulsars move along their jet axes. However, while the Crab and Vela pulsars both have transverse velocities of $\sim 130 \text{ km s}^{-1}$,

our results for PSR B0540-69.3 indicate a much higher value of $1190 \pm 560 \text{ km s}^{-1}$, assuming a distance to the LMC of 51 kpc. A third epoch of HST imaging is clearly needed to establish this result at a higher significance level.

This work has been partially supported by Russian Foundation of Basic Research (RFBR, grants 02-02-17668, 03-02-17423 and 03-07-90200), Russian Leading Scientific School (RLSS) program

1115.2003.2, and by The Royal Swedish Academy of Sciences. The research of PL is sponsored by the Swedish Research Council. PL is a Research Fellow at the Royal Swedish Academy supported by a grant from the Wallenberg Foundation. We also acknowledge support from the Swedish Research Council.

References

- [1] Manchester, R. N., Staveley-Smith, L., & Kesteven, M. J. The radio structure of supernova remnant 0540-69.3. *Astrophys. J.*, 411, 756-760, 1993.
- [2] Seward, F. D., & Harnden, Jr. F. R. The outer shell of SNR 0540-69.3. *Astrophys. J.*, 421, 581-584, 1994.
- [3] Gotthelf, E. V., & Wang, Q. D. A Spatially Resolved Plerionic X-Ray Nebula around PSR B0540-69. *Astrophys. J.*, 532, L117-L120, 2000.
- [4] Mathewson, D. S., Dopita, M. A., Tuohy, I. R., et al. A new oxygen-rich supernova remnant in the Large Magellanic Cloud. *Astrophys. J.*, 242, L73-L76, 1980.
- [5] Caraveo, P. A., Bignami, G. F., Mereghetti, S., et al. High-resolution optical imaging of the Large Magellanic Cloud plerion 0540 - 69. *Astrophys. J.*, 395, L103-L105, 1992.
- [6] Seward, F. D., Harnden, Jr. F. R., & Helfand, D. J. Discovery of a 50 millisecond pulsar in the Large Magellanic Cloud. *Astrophys. J.*, 287, L19-L22, 1984.
- [7] Middleditch, J., & Pennypacker, C. R. Optical pulsations in the large Magellanic Cloud remnant 0540-69.3. *Nature*, 313, 659-661, 1985.
- [8] Manchester, R. N., Mar, D. P., Lyne, A. G., et al. Radio detection of PSR B0540-69. *Astrophys. J.*, 403, L29-L31, 1993.
- [9] Chanan, G. A., Helfand, D. J., & Reynolds, S. P. An optical synchrotron nebula around the X-ray pulsar 0540-69.3 in the Large Magellanic Cloud. *Astrophys. J.*, 287, L23-L26, 1984.
- [10] Serafimovich, N. I., Shibanov, Yu. A., Lundqvist, P., et al. The young pulsar PSR B0540-69.3 and its synchrotron nebula in the optical and X-rays. *Astron. & Astrophys.* 425, 1041-1060, 2004.
- [11] Morse, J. A., Fesen, R. A., Chevalier, R. A., et al. Location of the Optical Reverse Shock in the Cassiopeia A Supernova Remnant. *Astrophys. J.*, 614, 727-736, 2004.
- [12] Tananbaum, H. Cassiopeia A. *IAU Circ.*, 7246, 1, Green, D. W. E. (Eds.), 1999.
- [13] Hwang, U., Petre, R., Holt, S. S., et al. The Thermal X-Ray-emitting Shell of Large Magellanic Cloud Supernova Remnant 0540-69.3. *Astrophys. J.*, 560, 742-748, 2001.
- [14] Morse, J. A. HST Observations of Young, Oxygen-Rich Supernova Remnants. *RewMexAA*, 15, 243-245, 2001.
- [15] Caraveo, P. A., Mignani, R. P., De Luca, A., et al. SNR0540-69-the Crab Twin-Revisited: Chandra vs. HST. *Livio, M. et al. (Eds.), A decade of HST science, 2000, Baltimore.* p.9 [astro-ph/0009035]
- [16] Serafimovich, N., Lundqvist, P., Sollerman, J., et al. Kinematics and structure of supernova remnant 0540-69.3. *Astron. & Astrophys.*, 2005, submitted
- [17] Kirshner, R. P., Morse, J. A., Winkler, P. F., et al. The penultimate supernova in the Large Magellanic Cloud - SNR 0540-69.3. *Astrophys. J.*, 342, 260-271, 1989.
- [18] Caraveo, P. A., Mignani, R. P. A new HST measurement of the Crab Pulsar proper motion. *Astron. & Astrophys.*, 344, 367-370, 1999.
- [19] Osterbrock, D. E. *Astrophysics of Gaseous Nebulae and Active Galactic Nuclei.* Univ. Sci. Books, California, 1989.
- [20] Lundqvist, P., & Fransson, C. The Line Emission from the Circumstellar Gas around SN 1987A. *Astrophys. J.*, 464, 924-942, 1996.
- [21] Ramsbottom, C. A., Bell, K. L., & Stafford, R. P. Effective Collision Strengths for Electron Impact Excitation of Singly Ionized Sulfur. *Atomic Data and Nuclear Data Tables*, 63, 57, 1996.
- [22] Davidson, K., & Fesen, R. A. Recent developments concerning the Crab Nebula. *Annual review of astronomy and astrophysics*, 23, 119-146, 1985.
- [23] Hill, R. J., Dolan, J. F., Bless, R. C., et al. The Spectrum of the Large Magellanic Cloud

- Pulsar B0540-69. *Astrophys. J.*, 486, L99-L102, 1997.
- [24] Middleditch, J., Pennypacker, C. R., & Burns, M. S. Optical color, polarimetric, and timing measurements of the 50 MS Large Magellanic Cloud pulsar, PSR 0540-69. *Astrophys. J.*, 315, 142-148, 1987.
- [25] De Luca, A., Mignani, R. P., & Caraveo, P. A. The Vela pulsar (PSR B0833-45) proper motion revisited with HST astrometry. *Astron. & Astrophys.*, 354, 1011-1013, 2000.
- [26] Maran, S. P., Sonneborn, G., Pun, C. S. J., et al. Physical Conditions in Circumstellar Gas Surrounding SN 1987A 12 Years after Outburst. *Astrophys. J.*, 545, 390-398, 2000.
- [27] Krabbe, A. C., & Copetti, M. V. F. Electron temperature fluctuations in 30 Doradus. *Astron. & Astrophys.*, 387, 295-300, 2002.
- [28] Pun, C. S. J., Michael, E., Zhekov, S. A., et al. Modeling the Hubble Space Telescope Ultraviolet and Optical Spectrum of Spot 1 on the Circumstellar Ring of SN 1987A. *Astrophys. J.*, 572, 906-931, 2002.